Design of a Two-Step Pulsed Pressure-Swing Adsorption-Based Oxygen Concentrator

V. Rama Rao, S. Farooq, and W. B. Krantz
Dept. of Chemical and Biomolecular Engineering, National University of Singapore, Singapore 117576

DOI 10.1002/aic.11953
Published online August 13, 2009 in Wiley InterScience (www.interscience.wiley.com).

A two-step pulsed pressure-swing adsorption (PPSA) process has been modeled to assess the extent to which an oxygen concentrator might be miniaturized for medical applications. The process consists of a single bed of packed adsorbent particles that is alternately pressurized and depressurized at the feed end. An enriched oxygen product is withdrawn at ambient pressure from the product end when the bed is pressurized at the feed end. The product end remains closed during depressurization. The model development addresses the manner in which axial dispersion enters into the describing equations and the formulation of proper boundary conditions, both of which have not been handled rigorously in some prior modeling studies. The describing equations are solved using COMSOL® Multiphysics software. The effect on the performance of the adsorption time, desorption time, bed length, particle diameter, and imposed pressure drop across the bed have been investigated. An interesting novel result is that for a chosen particle size, bed length, and applied pressure drop, there is an optimum combination of adsorption and desorption times that maximizes the product purity. The results suggest that there are operating windows for both 5A and partially Ag-exchanged Li-substituted 13X zeolite adsorbents wherein the product oxygen purity is greater than 90%. At a given product flow rate within this operating window, the extent of miniaturization is limited by the (maximum) cycling frequency that is practically achievable. Sizing of an oxygen concentrator for personal medical applications is also discussed. A principal conclusion is that a compact oxygen concentrator capable of producing a highly oxygen-enriched product is possible using commercially available adsorbents and implementable operating conditions. *AIChE J*, 56: 354–370, 2010
Keywords: portable oxygen concentrator, COPD, rapid cycling, air separation, 5A zeolite, 13X zeolite

Introduction

The use of an oxygen-enriched stream produced from air spans from classical chemical engineering to biological and medical applications. There is a significant demand for a portable oxygen supply for personal use by people needing oxygen therapy. Medical conditions in humans such as Chronic Obstructive Pulmonary Disease (COPD), limit the capacity of the lung to oxygenate blood by breathing atmospheric air. A constant supply of pure oxygen or oxygen-enriched air is essential to facilitate breathing for such patients.

One option for patients with COPD is to use a small oxygen cylinder for breathing. The other available option is to use a device that draws in air and produces varying degrees of enriched oxygen using pressure-swing adsorption (PSA) or membrane technology, which the patient with COPD can then use to facilitate their breathing. These options, due to

Correspondence concerning this article should be addressed to S. Farooq at chesf@nus.edu.sg

Table 1. Summary of Important Publications on RPSA Processes

Authors	Adsorbent/Adsorbate	Scope of Study
Turnock et al.[1]	5A zeolite/CH_4-N_2	Theoretical and experimental study of effect of process variables on performance; 1-bed, 2-step process with continuous production.
Jones et al.[2]	5A zeolite and activated carbon/ N_2—O_2, CH_4—N_2, CH_4—H_2, CO—H_2	Experimental study of effect of process variables on performance; 1-bed, 2 and 3-step process with continuous production.
Pritchard et al.[3]	5A zeolite/air separation	Experimental study of effect of process variables on separation performance; 1-bed, 3-step process with continuous production.
Sircar[4]	5A zeolite and activated carbon/ N_2—O_2CO_2—H_2, CH_4—H_2	Separation of binary gas mixtures in a single bed packed with two-shallow adsorbent layers; 2-step cycle with alternate production from the two layers.
Hart et al.[5]	5A zeolite and activated carbon/ CH_4—CO_2	Experimental and theoretical study comparing PPSA processperformance on two adsorbents; 1-bed, 3-step process with continuous production.
Alpay et al.[6]	5A zeolite/air separation	Modeling and simulation of RPSA process for air separation; 1-bed, 2-step process with continuous production.
Baron[7]	5A zeolite/air separation	Theoretical study of effect of diffusivity change on RPSA process performance; 1-bed, 3-step process with continuous production.
Lu et al.[8]	Activated carbon/H_2—CO	Theoretical study of binary gas separation in a RPSA Process; 1-bed, 3-step process having distinct pressurization, production, and depressurization steps.
Alpay et al.[9]	5A zeolite/air separation	Effect of adsorbent particle size on RPSA process performance; 1-bed, 2-step process with continuous production.
Kulish et al.[10]	Molecular sieves/air separation	Multibed RPSA process for air separation; 4-step cycle where the beds are coupled through pressure equalization.
Zhang et al.[11]	Silica gel/N_2—CO_2	Comparison of double bed and single bed RPSA process performance for heavy component recovery; 3-step process including a heavy reflux step.
Ackley et al.[12]	Oxysiv-7 and LiX/air separation	Design of lightweight medical oxygen concentrator; 2-bed, 6-step process where the beds are coupled through pressure equalization, product pressurization and purge steps.
Huang et al.[13]	5A Zeolite/air separation	Theoretical study comparing radial and axial RPSA processes; 1-bed, 3-step process with continuous production.
Todd et al.[14]	LiLSX/air separation	Comparison of two models with experiments;1-bed,4-step process.
Keefer et al.[15]	Laminated adsorbents/air separation	High frequency PSA/VPSA using laminated sheet adsorbers; 3-bed, 7-step process where the beds coupled though pressure equalization and purge steps.
Khiavi et al.[16]	Molecular sieves/H_2—CO_2	Effect of cycling frequency on the bed size; 3-bed, 5-step process where the beds are coupled through pressure equalization steps.

the size and weight of the devices, have limited portability that results in restricted mobility for patients who might otherwise be more physically active. Therefore, an oxygen-concentrating device using atmospheric air as feed that is sufficiently small in size and lighter in weight (and at the same time delivers $\geq$90% pure oxygen at a rate of 5 LPM required by the American Medical Association, AMA) can significantly improve the quality of life for those people who need oxygen therapy to overcome lung insufficiency.

An oxygen concentrator using PSA technology consists of one or more adsorption columns, a compressor and several valves to control the pressure cycling and flow sequence of atmospheric air fed to the system. The adsorption columns and the compressor are the two principal contributing factors to the size and weight of the device. The main issues for size and weight reduction are miniaturization of the adsorption column and the compressor. A principal focus in this study is miniaturization of the adsorption column.

The oxygen concentrators designed based on a conventional four-step Skarstrom PSA cycle suffer from multivalve switching and low separation efficiency per unit mass of adsorbent; therefore, they cannot be made very compact and lightweight. Although PSA units for concentrating oxygen from air have been developed for small scale medical applications, commercially available units are still not suitable for ambulatory use by a patient with active COPD. Therefore, a more compact and lightweight design for an oxygen concentrator has received attention to address the problems associated with its portability and efficiency, which in turn can significantly improve the quality of life for patients with COPD.

Pulsed pressure-swing adsorption (PPSA), one of the early advancements in PSA technology, replaces a four-step Skarstrom cycle with a two-step cycle involving only adsorption and desorption steps with pressure cycling at the feed end, which induces the pressure gradient along the bed during the adsorption step. The feed flow rate is determined by the imposed pressure gradient, adsorbent particle size, bed length, and the adsorption rate of the components from the feed. Thus, PPSA facilitates rapid cycling of the process and hence increases oxygen productivity per unit mass of adsorbent, which is essential for reducing the bed size and consequently the weight of the adsorption-based oxygen concentration device.

The idea of rapid cycling to reduce bed size has also been applied to multibed and multistep PSA processes including pressure equalization and purge steps. In the PSA literature, RPSA (rapid pressure swing adsorption) is used as a general name for PSA processes of all configurations that employ rapid cycling. Seminal studies on RPSA in the open and patent literature are summarized in Table 1. The earliest publication on a pulsed PSA process was by Turnock and Kadlec[1] who studied the performance of methane–nitrogen separation. They concluded that rapid cycling of the process significantly improved the nitrogen enrichment at the expense of low recovery. Jones and Keller[2] subsequently patented an RPSA process. They found that a short bed filled with small adsorbent particles (20–120 mesh) allowed faster cycling and

resulted in a substantially higher oxygen recovery. They demonstrated that rapid cycling resulted in a fivefold increase in the oxygen productivity per unit mass of adsorbent relative to the conventional Skarstrom PSA process. They also showed that a longer desorption time than the adsorption time was necessary for a proper regeneration of the bed prior to the subsequent cycle. The patent filed by Jones and Keller[2] in 1980 stimulated further work on RPSA. Prichard et al.[3] experimentally investigated the effect of process variables on the performance of an RPSA process for air separation using a 5A zeolite. They were able to attain 30% oxygen purity at an oxygen flow rate of 2 l/min using an RPSA device that weighted ~19 kg. Sircar[4] patented an RPSA process for the separation of binary mixtures such as oxygen–nitrogen, methane–nitrogen, and hydrogen–carbon dioxide that used a single adsorption column operating under rapid pressure cycling. Alpay et al.[6] developed a comprehensive theoretical model for an RPSA process and concluded that the separation capability of a pulsed RPSA process is the best for adsorption beds packed with 250–350 μm particles. Lu et al.[8] modeled a single bed RPSA process with complex dynamics and studied its performance under various initial and operating conditions. Kulish et al.[10] studied the design of an oxygen concentrator based on the RPSA principle. They used more than three sieve beds operated sequentially so that the time for adsorption was shorter than that for desorption of nitrogen. Ackley et al.[12] patented a medical oxygen concentrator design based on a very fast cycling PSA process. The oxygen concentrator had a bed size factor of ~0.14 kg adsorbent/kg O_2/day. Huang et al.[13] theoretically compared the performance of radial and axial RPSA processes for air separation. They also studied the effect of process variables on the performance of a radial RPSA process. They demonstrated that the radial RPSA process has the advantage of lower pressure drop for the same imposed pressure gradient, gas flow rate and adsorbent particle size compared to an axial RPSA process. Keefer et al.[15] have used a rotor-stator assembly to implement high frequency PSA and VSA cycles in a multibed arrangement. They have also demonstrated significant pressure drop reduction in laminated adsorbers. Khiavi et al.[16] studied the separation of hydrogen from syngas using an RPSA process. They used more than three adsorption columns, each compromised of at least one thin adsorbent sheet material with one or more adsorbents.

To gain an understanding of the size reduction achieved to date via rapid cycling, it is useful to note that in two patents entitled "Miniaturized Wearable Oxygen Concentrator" (Warren, 2002[17]; 2003[18]) two adsorbent beds were used, each of which consisted of a 0.05-m ID diameter pipe with a length of ~0.3 m. The lightest oxygen concentrator (Inogenone®) currently available for personal use by active people needing oxygen therapy weighs ~5 kg and has the size of a small desktop computer.

The idea of ultra rapid pressure-swing adsorption (URPSA) in fact is an extension of the RPSA concept whereby a very thin bed of adsorbent particles is subjected to pressure cycling at one end at a high frequency in order to further enhance the adsorbent productivity. The only published work on URPSA is by Kopaygorodsky et al.[19] which is a simulation study of a two-step high frequency pressure cycling between 1 and 1.5 atm pressure at the feed end of a 2-mm-thick adsorbent bed packed with a 1 μm adsorbent. The study introduces an interesting idea but does not exploit its full potential.

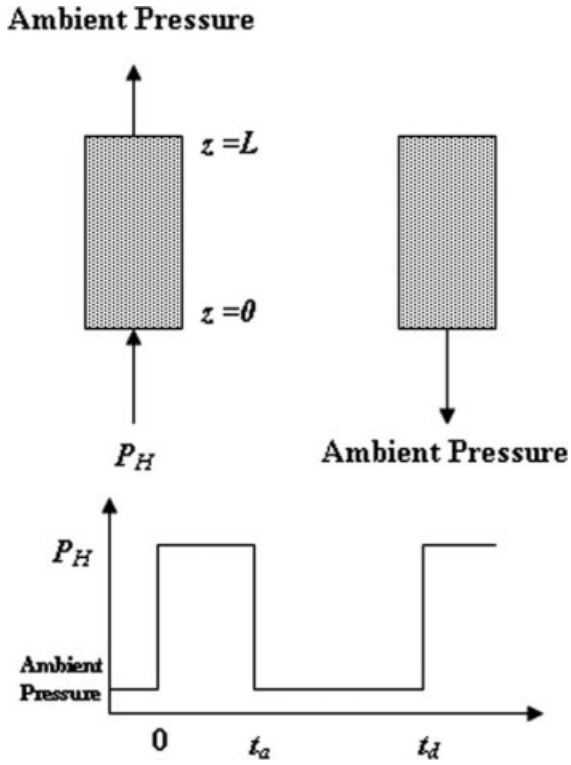

Figure 1. Schematic representation of a two-step pulsed pressure-swing adsorption process.

Among the configurations used in the RPSA studies summarized in Table 1 and reviewed earlier, the two-step PPSA process is the simplest in terms of instrumentation required to implement the cycling. It can also be extended to multiple bed arrangement in order to make the feeding and light product delivery continuous without introducing any additional coupling among the adsorbers. These features are essential to develop an adsorption based oxygen concentrating device that is sufficiently small in size and light in weight for portable personal medical applications, such as mobile use by physically active patients with COPD. For these reasons, a two-step PPSA process, schematically shown in Figure 1, has been chosen in the present study. In the published two- and three-step PPSA studies, the product withdrawal was continued while the bed was depressurized at the feed end. In contrast, the product end is kept closed during the desorption step in this study. As a result, the desorbing oxygen is partially conserved in the product end and partially used to self-purge the feed end of the adsorber. A detailed analysis of this process has led to the following advances not addressed in other publications:

Performance is maximized for oxygen purity by optimizing the duration of both the adsorption and desorption steps for a wide range of bed lengths, adsorbent sizes, and amplitude of the pressure cycling covering the domain of both RPSA and URPSA operation.

Understanding of the practical constraints that limit PPSA process miniaturization.

Generalized plots are developed for designing a PPSA oxygen concentrator for two promising commercial nitrogen-selective adsorbents that relate adsorbent volume to the process variables (bed length, particle diameter, operating pressure, optimum adsorption, and desorption times) for producing oxygen from air at any desired purity at a target production rate including AMA standards for personal medical applications.

Model Development

Process description

The pulsed pressure-swing adsorption process (PPSA) consists of a single fixed bed packed with adsorbent particles considerably smaller in diameter than those used in conventional PSA. The PPSA cycle involves two steps: adsorption and desorption. A schematic of a single bed PPSA process is shown in Figure 1. During a typical adsorption step for air separation, the feed end of the column ($z = 0$) is supplied with high pressure air and the product end ($z = L$) is kept open to the atmosphere. As a result of the pressure difference across the column, high pressure air flows through the adsorbent bed from the feed to the product end. In this step nitrogen is removed by preferential adsorption and a product enriched in the less strongly adsorbed oxygen is withdrawn at atmospheric pressure from the product end of the column. During the desorption step, the product end is closed and the feed end is opened to the atmosphere. In this step, the strongly adsorbed nitrogen is desorbed into the gas phase due to the rapid reduction in pressure in the bed and the desorbed gas, enriched in nitrogen, exits at the feed end of the column. The duration of both the adsorption and desorption steps affects the oxygen product purity.

Mathematical modeling

In developing a mathematical model for the PPSA process, the following assumptions are made:

Ideal gas conditions apply.

The system is assumed to be isothermal.

Gas flow in the adsorbent bed is described by Darcy's law.

Adsorption equilibrium between the gas and adsorbed phase is described by a binary Langmuir isotherm model with parameters obtained from single component data.

A linear driving force (LDF) approximation describes the gas transport in the adsorbent.

The feed is approximated as a mixture of nitrogen and oxygen only in the ratio of 79:21.

Uniform particle size and bed voidage are assumed.

The molecular weight of the gas is assumed to be constant along the bed length.

The gas viscosity is assumed to be independent of pressure.

Model equations

As a pressure difference is imposed across the adsorption column, compressible gas effects must be incorporated into the describing equations. This introduces some subtleties in developing the describing equations, in particular with respect to the proper formulation of the axial dispersion and boundary conditions. For this reason, the describing equations will be developed in terms of the molar fluxes and subsequently expressed in terms of the partial and total pressures.

The equations of continuity for the nitrogen (component A) and oxygen (component B) are given by

$$\frac{\partial c_A}{\partial t} = -\frac{\partial N_A}{\partial z} - \left(\frac{1-\varepsilon}{\varepsilon}\right)\frac{\partial \bar{q}_A}{\partial t} \tag{1}$$

$$\frac{\partial c_B}{\partial t} = -\frac{\partial N_B}{\partial z} - \left(\frac{1-\varepsilon}{\varepsilon}\right)\frac{\partial \bar{q}_B}{\partial t} \tag{2}$$

where N_i C_i and $\overline{q}_i$ denote the molar flux with respect to a stationary reference frame, the molar concentration, and the molar adsorption per unit volume of adsorbent, respectively, of component i (A or B); the overbar denotes the average adsorbed concentration over the volume of the particles; ε denotes the voidage or void fraction in the adsorbent bed; and t and z are the temporal and spatial coordinates, respectively.

The appropriate form of Fick's law must incorporate axial dispersion relative to the interstitial velocity, u_z, through the porous media and hence is given for the two components by

$$N_A = -cD_L\frac{\partial y_A}{\partial z} + y_A(N_A + N_B) = -cD_L\frac{\partial y_A}{\partial z} + c_A u_z \tag{3}$$

$$N_B = -cD_L\frac{\partial y_B}{\partial z} + y_B(N_A + N_B) = -cD_L\frac{\partial y_B}{\partial z} + c_B u_z \tag{4}$$

where $c = c_A + c_B$ is the molar density and D_L is the axial dispersion coefficient defined relative to the interstitial velocity. Note that Fick's law must be defined in terms of the mole fraction driving force to insure that $N_A + N_B = cu_z$. Some prior studies have not properly accounted for the required compatibility between the axial dispersion coefficient and form of Fick's law.[6,20–24]

The molar adsorption rates are given by

$$\frac{\partial \bar{q}_A}{\partial t} = k_A\left(q_A^e - \bar{q}_A\right) \tag{5}$$

$$\frac{\partial \bar{q}_B}{\partial t} = k_B\left(q_B^e - \bar{q}_B\right) \tag{6}$$

in which k_i and q_i^e are the mass-transfer coefficient and equilibrium adsorbed molar concentration per unit adsorbent volume, respectively, for component i (A or B). The equilibrium molar adsorption is assumed to be described by the multicomponent Langmuir adsorption isotherm:

$$\frac{q_A^e}{q^\infty} = \frac{b_A c_A}{1 + b_A c_A + b_B c_B} \tag{7}$$

$$\frac{q_B^e}{q^\infty} = \frac{b_B c_B}{1 + b_A c_A + b_B c_B} \tag{8}$$

in which q^∞ is the saturation molar adsorbed concentration per unit adsorbent volume and b_i is the Langmuir constant for component i (A or B).

The interstitial gas velocity through the porous media is related to the local pressure gradient via Darcy's law:

$$u_z = -\frac{k_p}{\mu}\frac{\partial P}{\partial z} \tag{9}$$

in which μ is the shear viscosity and k_p is the bed permeability described by the Blake-Kozeny equation as follows:

$$k_p = \frac{d_p^2}{150}\left(\frac{\varepsilon}{1-\varepsilon}\right)^2 \tag{10}$$

The overall equation of continuity is obtained by adding the equations of continuity for the two species, Eqs. 1 and 2, while recognizing the implications of Eqs. 3 and 4:

$$\frac{\partial c}{\partial t} = -\frac{\partial (cu_z)}{\partial z} - \left(\frac{1-\varepsilon}{\varepsilon}\right)\frac{\partial}{\partial t}(\bar{q}_A + \bar{q}_B) \tag{11}$$

Note that there is no axial dispersion term in the overall continuity equation. Some prior studies of PSA[6,20–24] have included an axial dispersion term in the overall continuity equation. This is consequence of not employing a form of Fick's law that is consistent with the dispersion being relative to the interstitial velocity through the porous media.

Only two of the three equations given by Eqs. 1, 2, and 11 are independent. Here we will choose Eqs. 1 and 11, the nitrogen and overall continuity equations, respectively. When Eqs. 1 and 3 are combined and the ideal gas law is used to simplify the resulting equation as well as Eq. 11, these equations assume the following form in terms of the partial and total pressures:

$$\frac{\partial p_A}{\partial t} = D_L\frac{\partial}{\partial z}\left[P\frac{\partial}{\partial z}\left(\frac{p_A}{P}\right)\right] - \frac{\partial}{\partial z}(p_A u_z) - RT\left(\frac{1-\varepsilon}{\varepsilon}\right)\frac{\partial \bar{q}_A}{\partial t} \tag{12}$$

$$\frac{\partial P}{\partial t} = -\frac{\partial}{\partial z}(Pu_z) - RT\left(\frac{1-\varepsilon}{\varepsilon}\right)\frac{\partial}{\partial t}(\bar{q}_A + \bar{q}_B) \tag{13}$$

Each of Eqs. 12 and 13 requires an initial and two boundary conditions and each of Eqs. 5 and 6 requires an initial condition. The boundary conditions are different for the adsorption (pressurization) and desorption (depressurization) steps. The initial condition for the adsorbent bed is assumed to be equilibrium with air having a nitrogen mole fraction y_{A0} at the prevailing pressure P_L:

$$\left.\begin{array}{l} p_A = y_{A0}P_L \\ P = P_L \\ \bar{q}_A = q_A^e|_{p_A} \\ \bar{q}_B = q_B^e|_{p_B} \end{array}\right\} \quad \text{at} \quad t = 0, \;\; 0 \le z \le L \tag{14}$$

At each end of the column the following conditions apply for component i (A or B) during both the adsorption and desorption steps:

$$N_i|_{z=0^-} = \varepsilon\, N_i|_{z=0^+} \quad \text{at} \quad z = 0 \tag{15}$$

$$\varepsilon\, N_i|_{z=L^-} = N_i|_{z=L^+} \quad \text{at} \quad z = L \tag{16}$$

If Eqs. 15 and 16 are written for each component, the resulting component equations at each end of the column can be added to obtain the appropriate boundary conditions for the overall continuity equation. When Eqs. 3 and 4 are substituted for the molar fluxes and the ideal gas law is used to express the concentrations, molar density and mole fractions in terms of the partial and total pressures, the boundary conditions assume the following form:

$$\left.\begin{array}{ll} -PD_L\frac{\partial}{\partial z}\left(\frac{p_A}{P}\right) & = u_z(y_{A0}P_H - p_A) \\ P = P_H & \end{array}\right\}$$

$$\text{at} \quad z = 0^+ \quad n(t_a + t_d) \le t \le (n+1)t_a + nt_d \tag{17}$$

$$\left.\begin{array}{l} \frac{\partial}{\partial z}\left(\frac{p_A}{P}\right) = 0 \\ P = P_L \end{array}\right\} \quad \text{at} \quad z = 0^+$$

$$(n+1)t_a + nt_d \le t \le (n+1)(t_a + t_d) \tag{18}$$

$$\left.\begin{array}{l} \frac{\partial}{\partial z}\left(\frac{p_A}{P}\right) = 0 \\ P = P_L \end{array}\right\} \quad \text{at} \quad z = L^- \quad n(t_a + t_d) \le t \le (n+1)t_a + nt_d \tag{19}$$

$$\left.\begin{array}{l} \frac{\partial}{\partial z}\left(\frac{p_A}{P}\right) = 0 \\ \frac{\partial P}{\partial z} = 0 \end{array}\right\} \quad \text{at} \quad z = L^-$$

$$(n+1)t_a + nt_d \le t \le (n+1)(t_a + t_d) \tag{20}$$

Equations 17 and 18 give the boundary conditions for the species continuity and overall continuity equations at the end of the column defined by $z = 0$ during the adsorption and desorption steps, respectively. Equations 19 and 20 give the boundary conditions for the species continuity and overall continuity equations at the end of the column defined by $z = L$ during the adsorption and desorption steps, respectively. These boundary conditions involve no approximations other than those summarized at the beginning of this model development. Note that some prior PSA modeling studies[25] involving compressible gas flow have assumed that the derivative of the partial pressure is zero at the end of the column defined by $z = L$; Eqs. 19 and 20 indicate that it is the derivative of the mole fraction that is zero at $z = L$.

Equilibrium and kinetic parameters

Two adsorbents, namely 5A and partially Ag-substituted Li-X zeolite ($Li_{94.2}Na_{0.7}Ag_{1.1}$-X-1.0 referred to as Ag-Li-X), were used to study the performance of the two-step PPSA process for oxygen enrichment from air. Table 2 summarizes the equilibrium data for both adsorbents taken from published sources.[26,27] Other common operating parameters are summarized in Table 3.

Table 2. Equilibrium Isotherm Parameters for 5A* and Li-Ag-X ($Li_{94.2}Na_{0.7}Ag_{1.1}$-X-1.0)† Zeolites

Parameter‡	5A	Ag-Li-X
q^∞ (mol/cc)	5.23×10^{-3}	3.1618×10^{-3}
b_A (cc/mol)	2813.7	28613
b_B (cc/mol)	893.5	2204.5

*Farooq et al.[26]
†Hutson et al.[27]
‡A is nitrogen and B is oxygen.

Table 3. Common Parameters Used in the Simulations

Process Parameter	Range
Feed Air	79:21 N_2:O_2
Bed voidage(ε)	0.33
Particle voidage(ε_p)	0.35
Gas constant (R)	82.05 atm cc/mol K
Temperature	298.15 K
Product pressure (P_L)	1 atm
Reference pressure (P_R)	1 atm
Feed pressure (P_H)	1.5–10.5 atm
Adsorbent size (d_p)	0.001–0.04 cm
Bed length (L)	0.4–600 cm
Molecular diffusivity (D_M)	0.204 cm^2/s
Viscosity of air (μ)	1.8×10^{-10} atm s
Adsorbent particle density	1.20 g/cc

The rate of mass transfer between the gas phase and solid is approximated using the linear driving force (LDF) model, which is an effective approximation for equilibrium-controlled processes such as air separation via a 5A zeolite. Ruthven et al.[28] concluded that the macro-pore resistance controls the rate of intraparticle mass transfer, which is also the controlling step in the inter-phase mass transfer, in the case of zeolite-based air separation. The LDF mass-transfer rate constants for both nitrogen and oxygen have been calculated from the following approximation:

$$k_i = \Omega \frac{\varepsilon_p D_p}{r_p^2} \left(\frac{c}{q}\right)_i \quad \text{where } i = \text{A or B} \tag{21}$$

where D_p is the macropore diffusivity and Ω is an empirical parameter that can depend on the cycle time for faster cycling processes. The value $\Omega = 15$ is recommended for the macropore resistance for long contact times in a PSA process. A limiting value of $\Omega = 15$ is also found adequate for the current study based on the correlation established by Raghavan et al.[29] The macropore diffusivity (D_p) was related to the molecular diffusion coefficient assuming that the tortuosity factor (τ) was 3, as suggested by Farooq et al.,[26] who also suggested a value of 0.33 for particle porosity (ε_p). The effect of Knudson diffusion on the macropore diffusivity is neglected since the pressure is always above atmospheric in the present study:

$$D_P = \frac{D_M}{\tau} \tag{22}$$

where D_M is the molecular diffusivity of the oxygen-nitrogen pair at the average column pressure, P_{avg} ($= (P_H + P_L) / 2$), estimated from the Chapman-Enskog equation given in Bird et al.[30] In the LDF approximation the external film resistance is also relatively negligible compared with the macro resistance. In the limit of no flow, the Sherwood number $k_f d_p / D_M = 2$, which implies that the minimum value of $k_f = D_M / r_p$. Based on an order-of-magnitude analysis the external film resistance is about 50% of the macropore resistance in the limit of no-flow and it is even less in an actual PPSA operation.

The effective axial dispersion coefficient has been estimated from the correlation given by Ruthven[31]:

$$D_L = \gamma_1 D_M + \gamma_2 d_p \bar{u}_z \tag{23}$$

where γ_1 and γ_2 are constants whose typical values are 0.7 and 0.5, respectively, and the average interstitial velocity $\bar{u}_z$ is obtained from Darcy's law in combination with the Blake-Kozeny equation given by Eqs. 9 and 10 for a constant imposed pressure drop along a fixed bed length.

Numerical simulation

Equations 12 and 13, the species and overall continuity equations, respectively, expressed in terms of the partial and total pressures in the gas phase are coupled with the solid phase loading through Eqs. 5 and 6, and with the interstitial gas velocity through Eq. 9. Equations 7 and 8 are the adsorption equilibrium isotherm relationships for nitrogen and oxygen.

The set of coupled partial differential equations (PDEs) was solved using the COMSOL Multiphysics® (formerly FEMLAB®) software package. This software is a dynamic tool that uses the finite element method to solve partial differential equations encountered in real world engineering and scientific problems. It has several basic application modes related to various fields of engineering and science. It uses the integral approach to conservation, which does not suffer from Gibbs instability. The integral approach to conservation makes the code stable against any abrupt change/shock. To solve the aforementioned set of equations, the coefficient form of the PDE modes under COMSOL Multiphysics® in Application Modes was used. The equations describing the adsorption and desorption steps were set up and solved in COMSOL Multiphysics. The number of mesh elements was increased until the bed profiles and process performance indicators showed no further change. A grid of 960 mesh elements was used in the axial direction. The outputs from COMSOL Multiphysics were exported to MATLAB® at the end of each step. The cycling procedure was coded in MATLAB, which controlled the cycling and plotted the profiles at the end of each step for every cycle. Starting from the initial condition of an adsorbent bed saturated with respect to feed air at atmospheric pressure, the partial and total pressure, and velocity profiles in the fluid phase, and adsorbate loading profiles in the adsorbent phase evolved in time until reaching a cyclic steady-state. This implies that the instantaneous partial and total pressure profiles are identical during each successive cycle. A change in oxygen purity by $\leq 0.1\%$ in 5 cycles was used as the criteria to confirm cyclic steady-state. Depending on the parameter values, it required simulating 50–220 cycles to ensure the aforementioned cyclic steady-state criteria.

To assess the accuracy of COMSOL Multiphysics, the results were compared with an in-house simulation coded in FORTRAN® wherein orthogonal collocation was applied to convert the system of PDEs to a system of ordinary differential equations (ODEs) in time. Figure 2, which shows the oxygen partial pressure, total pressure, and velocity profiles for cyclic operation, confirms quantitative agreement between the predictions of the two simulators. For the same conditions the time required in COMSOL was on the order of 0.6–0.7 min/cycle as opposed to 7–8 min/cycle using the in-house simulator.

Simulation Results and Discussion

Performance of the PPSA process was analyzed based on the product purity, recovery, and productivity. Purity is the

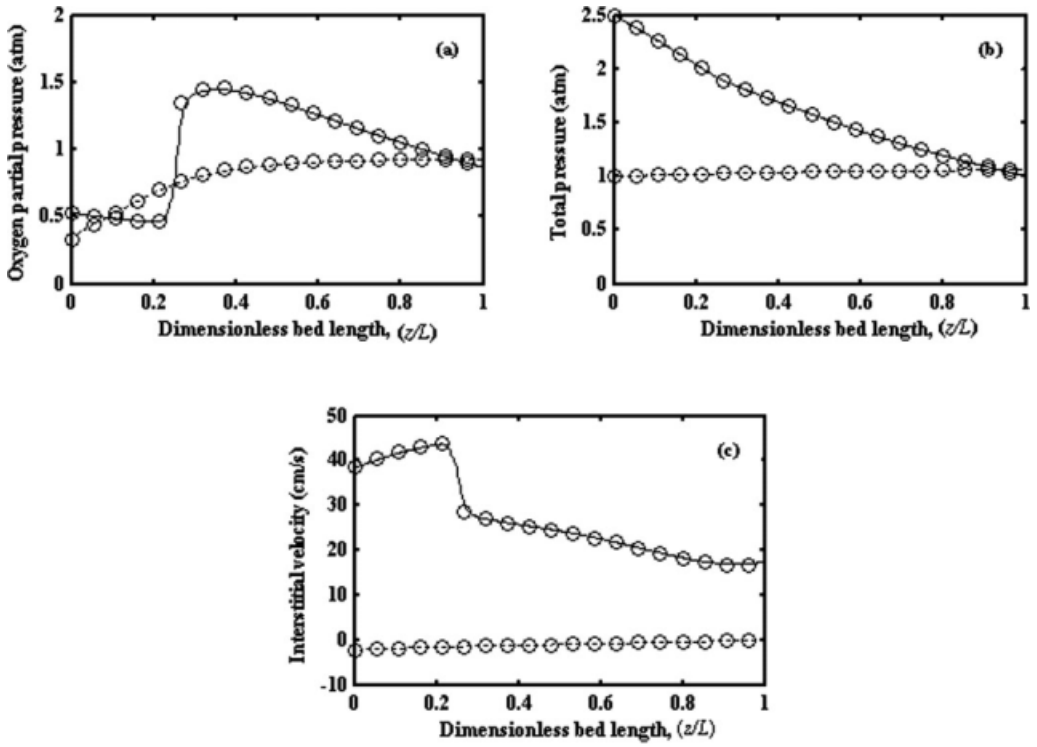

Figure 2. Comparison of bed profiles obtained from COMSOL multiphysics software (—— adsorption and – – – – desorption) and an in-house simulator (o) for (a) oxygen partial pressure, (b) total bed pressure and (c) interstitial velocity in gas phase at the end of adsorption and desorption steps after reaching cyclic steady-state.

The process parameters are $L = 2$ cm, $d_p = 0.002$ cm, $\Delta P = 1.5$ atm. Optimum adsorption and desorption times are 0.12 s and 1.2 s, respectively.

average oxygen mole fraction in the product stream delivered during the adsorption step. Recovery is defined as the ratio of the moles of oxygen in the product stream to the moles of oxygen fed to the column during the adsorption step. Productivity is defined as the volume of oxygen product delivered in the adsorption step per unit volume of adsorbent per unit time.

It should be noted that oxygen and argon adsorption isotherms are indistinguishable for the two nitrogen selective adsorbents used in this study. Hence, all the simulation results for oxygen purity have been scaled down by a factor of 21/22 in order to account for the presence of argon when atmospheric air is used as the feed. Atmospheric air also contains water vapor and CO_2 in trace amounts, which have been neglected in the simulations. Since zeolites have very strong affinity for water vapor and CO_2, the recommendation is to remove these trace components separately using a periodically replaceable filter before the PPSA unit. Therefore, neglecting water vapor and CO_2 in the simulation is justifiable.

Before presenting the findings from this simulation study, it is also important to discuss the impact of the assumptions related to adsorption heat effect, binary equilibrium calculation and intra-adsorbent gas transport.

The heat effect should be assessed for a PPSA process being developed for mobile use by physically active patients who need oxygen therapy. For such applications, typically small-diameter adsorbers (1–2 cm in diameter) will be used where high ratio of heat transfer area to packed volume will allow fast dissipation of the heat of adsorption and keep the temperature rise to a minimum. Hence, isothermal assumption is reasonable.

The extended Langmuir isotherm model based on single component parameters has been used in the simulation. Oxygen and nitrogen molecules are very similar in size and their saturation capacities are close enough to force an average saturation capacity without affecting the fit of the single component data in the range of interest. This makes the extended Langmuir isotherm thermodynamically consistent. There is no evidence to suggest that interaction between two nonpolar gases like oxygen and nitrogen can give rise to any significant nonideality to impair the predictions from this simulation study.

Although the pore diffusion model is a more realistic representation of the intra-adsorbent gas transport, several studies[28] have shown that difference between the pore diffusion model and LDF approximation in a cyclic process simulation can be minimized by adjusting Ω (see Eq. 21). A number of correlations for adjusting Ω have been proposed in the literature as a function of the dimensionless cycle time, θ, The ones that are based on analytically comparing particle uptake have used linear isotherms. Correlations based on direct comparison of PSA simulation results have used different degrees of isotherm nonlinearity. It is generally agreed that a

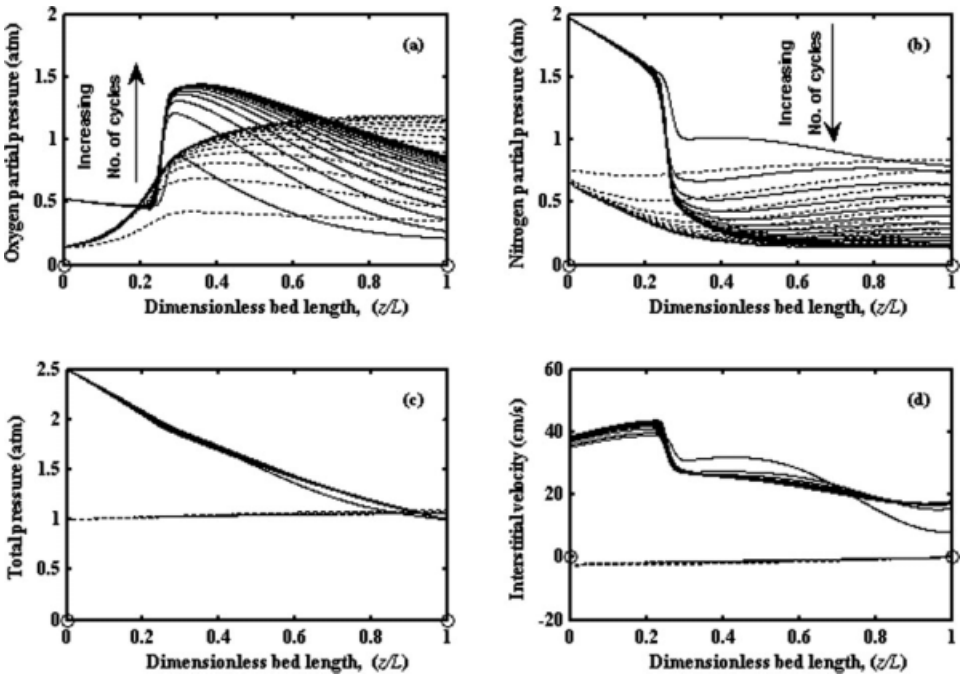

Figure 3. Profiles for (a) oxygen partial pressure, (b) nitrogen partial pressure, (c) total column pressure and (d) interstitial velocity in the gas phase plotted against dimensionless bed length showing approach to cyclic steady-state.

Starting from the 1st cycle, profiles from every 5th cycle are shown for 5A zeolite. The process parameters are $L = 2$ cm, $d_p = 0.002$ cm and $\Delta P = 1.5$ atm. Optimum adsorption and desorption times are 0.12 s and 1.2 s, respectively.

constant value $\Omega = 15$ works well when $\theta \geq 1.0$ for both linear and nonlinear isotherms. More recently, Todd and Webley[15] have shown excellent agreement between the LDF model with $\Omega = 15$ and pore diffusion model predictions for RPSA air separation on LiLSX in the range $\theta \geq 1.0$. These authors came to the same conclusion based on particle uptake study in an earlier publication.[32] The θ values are well above 1 for most of the other operating conditions simulated in this study. For one or two exceptional cases, the values for oxygen are still >1 and the nitrogen values lie between 0.1 and 1. Hence, the use of Eq. 21 with $\Omega = 15$ in the present study is a quantitatively reliable representation of the macropore controlled intraparticle diffusional transport of oxygen and nitrogen in the two adsorbents.

The PPSA performance depends on several process parameters such as the duration of the adsorption and desorption steps, adsorbent particle diameter, pressure drop across the column and bed length. The influence of these parameters is discussed in the following sections.

Dynamics of adsorption and desorption

The oxygen and nitrogen partial pressure, total pressure, and interstitial velocity profiles within the adsorption bed plotted at the end of the first step and every fifth step thereafter until reaching cyclic steady-state operation are shown in Figure 3. COMSOL Multiphysics in conjunction with MATLAB also allows tracking the evolution of various bed profiles within the duration of each step. Such visualization capability helps to physically understand and gain insight into the process. The sharp drop in partial pressure of nitrogen in Figure 3b is due to the rapid (selective) nitrogen adsorption at the feed end of the bed, which results in the sharp rise in oxygen partial pressure ahead of the nitrogen front observed in Figure 3a. The increase in velocity near the feed end of the bed, shown in Figure 3d, is due to the total pressure gradient near the bed entrance where the adsorbed phase is in equilibrium with feed air. The subsequent decrease in velocity is due to nitrogen adsorption exceeding the opposing effect of pressure gradient. During the desorption step the feed end is opened to the atmosphere and the product end is closed. By tracking the total pressure profile within the duration of the desorption step, it was observed that a pressure maximum occurs inside the bed whereby a pressure wave travels in both directions before near atmospheric pressure is attained throughout the bed. As the product end is closed during this step, this wave can cause the pressure at the product end to rise above atmospheric, which explains the pressure gradient from outlet to inlet seen in Figure 3c at the end of the desorption step. The residual (reverse) gradient of pressure at the end of the desorption step depends on the duration of this step. It is evident from Figures 3a, b that during the desorption step, both nitrogen, and oxygen are released from the adsorbed phase. Gas desorbed from the region behind the penetration of the adsorption front is rich in nitrogen and quickly exits through the bed inlet. In the region ahead of the penetration of the adsorption front, the desorbing gas is rich in oxygen and is conserved in the gas phase by preventing its excessive release through the inlet, which contributes to the product purity in the subsequent cycle. It is also evident from the profiles in Figure 3 that while the dynamics of the total

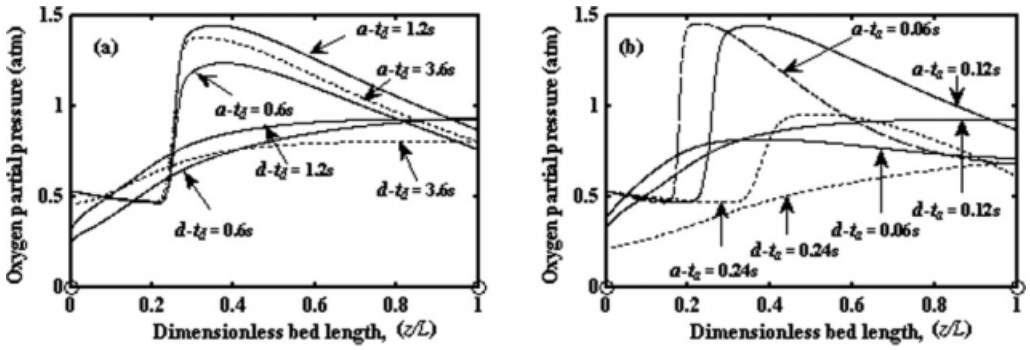

Figure 4. Effect of (a) desorption time and (b) adsorption time on the cyclic steady-state oxygen partial pressure profile along a 5A zeolite adsorbent bed for the adsorption and desorption step durations fixed at 0.12 s and 1.2 s, respectively.

Other operating parameters are $L = 2$ cm, $d_p = 0.002$ cm and $\Delta P = 1.5$ atm. See notation list for explanation of the legends used for the cyclic steady-state oxygen partial pressure profiles. $a - t_a$

column pressure are very fast and reach cyclic operation within a few cycles, the partial pressure profiles of both the gases require a large number of cycles to converge to cyclic steady-state operation. Lu et al.[5] have reported similar behavior for a three-step RPSA process where a hold step was introduced between the adsorption and desorption steps. The specific criterion used to confirm cyclic steady-state in this study is detailed in the ''Numerical simulation'' section.

Optimum in adsorption time and desorption time

Oxygen product purity from a pulsed PSA process using 5A zeolite and Ag-Li-X zeolite as the adsorbents was maximized by optimizing the duration of the adsorption and desorption steps for every set of operating parameters. It was interesting to note that there was an optimum combination of adsorption and desorption step durations at which the oxygen product purity becomes maximum for each set of operating parameters. To understand this phenomenon, the oxygen and nitrogen partial pressure profiles in the bed at the end of the adsorption and desorption steps after reaching cyclic steady-state operation were studied by varying either the desorption or the adsorption step duration while keeping the other constant; the results are shown in Figure 4. The purpose of the adsorption step is to preferentially remove as much nitrogen from the incoming feed air as possible near the feed end of the adsorption bed and push enriched oxygen towards the product end. But the purity of the oxygen product obtained in the adsorption step is also dependent on the state of the gas phase composition at the end of the desorption step in the previous cycle. In a conventional four-step PSA cycle, an external purge using raffinate product sweeps the bed voids clean of the preferentially extracted component of the feed that is desorbed from the adsorbent due to pressure reduction and at the same time promotes further desorption of the extract. It was discussed in relation to the results shown in Figure 3 that during desorption in a two-step PPSA process, oxygen-rich gas desorbed from the product end flows towards the open feed end thus creating a self-purge effect. For a given adsorption time, a very short desorption step means that desorbed oxygen does not have enough time to sufficiently sweep the bed and a large amount of nitrogen is left behind in the voids of the bed near the feed end. The residual nitrogen reduces the purity of the oxygen product in the subsequent adsorption step. A very long desorption time, on the other hand, results in an excessive loss of desorbed oxygen that outweighs the additional nitrogen capacity that might be created at the feed end of the bed as a result of the longer self-purge. The consequence is also a drop in oxygen product purity. These observations are evident from Figure 4a. Therefore, there is an optimum desorption time that maximizes the conservation of enriched oxygen desorbed from the product end without compromising nitrogen purging. The results in Figure 4b show the effect of changing the adsorption time for a fixed desorption time. The volume of gas fed to the adsorber is controlled by the duration of the adsorption step when all other operating conditions are held constant. Increasing the adsorption time increases the penetration of the adsorption wave front deeper into the bed as can be clearly seen in Figure 4b. Because a pressure drop is imposed along the bed length during the adsorption step, an advancing adsorption front also means a decreasing driving force for mass transfer. As such, a very long adsorption step pushes unadsorbed nitrogen toward the product end and reduces the oxygen product purity. In contrast, a very short adsorption time limits the penetration of the adsorption front. Although there is a sharp rise in the oxygen concentration ahead of the adsorption front, the zone of high purity oxygen remains confined to the middle of the bed since the allowed adsorption time is insufficient for it to reach the product end. Therefore, the optimum adsorption step duration maximizes the oxygen product purity by regulating the penetration of the mass-transfer front. A balance is struck such that the oxygen-rich zone reaches the product end, but limits nitrogen contamination resulting from a reduced driving force at the leading edge of the advancing mass-transfer front. Trends similar to those in Figure 4 were also observed in case of the Ag-Li-X zeolite.

All the process performance results presented in the subsequent sections are for the optimum combination of the adsorption and desorption step times for the corresponding set of process variables. A thorough manual search using small time step increments was conducted in order to determine the optimum adsorption and desorption step durations

$[(t_a)_{ref}, (t_d)_{ref}]$ for a set of (base case) process variables. To determine the optimum adsorption time for another combination of process variables, Eq. 24 was used to calculate a good first approximation $(t_a)_{current}$ based on the assumption that the optimum adsorption time is proportional to the average residence time of the feed gas in adsorption column under nonadsorbing conditions:

$$\frac{\left(\frac{L}{\overline{u}_z}\right)_{current}}{\left(\frac{L}{\overline{u}_z}\right)_{ref}} = \frac{(t_a)_{current}}{(t_a)_{ref}} \tag{24}$$

where $\overline{u}_z$ is the average interstitial gas velocity calculated using Darcy's law in combination with the Blake-Kozeny equation given by Eqs. 9 and 10, respectively. Use of the Blake-Kozeny equation to calculate the average interstitial velocity under nonadsorbing conditions permitted calculating a first approximation of the new optimum adsorption time for a change in any one or more of the process parameters, namely the imposed pressure drop, adsorbent particle size, and bed length. Note that the Blake-Kozeny equation assumes a linear pressure gradient in the bed, which is a good approximation for the computed total pressure profiles under the adsorption conditions shown in Figure 3. The first approximation of the new optimum desorption time was obtained by equating $(t_a/t_d)_{current}$ to $(t_a/t_d)_{ref}$. Starting from the first approximation, the adsorption and desorption times were varied further to obtain the optimum combination that maximized the oxygen product purity for the chosen new combination of operating parameters.

Generalizing the simulation results

To generalize the results from the numerical simulations, the possibility of correlating the process performance indicators in terms of dimensionless groups consisting of the process parameters was investigated. The set of Eqs. 5 through 9 and Eqs. 12 through 23 were made dimensionless by using appropriate scale factors[33] in order to obtain the minimum parametric representation in terms of eleven dimensionless groups as shown in the Appendix. Hence, the oxygen product purity, recovery and productivity will be functions of the eleven dimensionless groups identified in Eq. A26 and defined in the Appendix. Note that the groups, Π_2, Π_3, Π_5, Π_6, Π_8, Π_{11}, are dependent only on adsorbent properties, composition and physical properties of the feed gas, product delivery pressure, and temperature. Therefore, for air separation using a specified adsorbent, product delivery pressure and temperature, the oxygen product purity, recovery and productivity will be functions of only the five dimensionless groups Π_1, Π_4, Π_7, Π_9, and Π_{10}. The particle diameter, ratio of particle diameter to bed length and maximum pressure have been isolated into the dimensionless groups Π_1, Π_4, and Π_7, respectively, whereas the adsorption and desorption times have been isolated into the dimensionless groups Π_9 and Π_{10}, respectively. In the "Optimum in adsorption time and desorption time" section, it was observed that the oxygen product purity is maximum for an optimum combination of adsorption and desorption step durations for a specified bed length, adsorbent particle size and pressure drop. Once the oxygen product purity is maximized with respect to the durations of the adsorption and desorption steps for a given set of process parameters, the process performance becomes independent of dimensionless groups Π_9 and Π_{10}; this follows from the fact that the maximization introduces two additional independent equations that can be used to eliminate Π_9 and Π_{10}. Hence, for a fixed adsorbent delivering an oxygen-enriched product at atmospheric pressure the maximum oxygen purity depends only on the three dimensionless groups Π_1, Π_4 and Π_7. Therefore, the PPSA process performance was computed in terms of the three dimensionless groups Π_1, Π_4, and Π_7 over an extensive range of values summarized in Table 4 that cover the full domain of the PPSA process operation including URPSA. Correlating the process performance indicators, oxygen product purity, recovery, and productivity, with the aforementioned dimensionless groups will guide the designer in selecting a proper set of process parameters for a specific application. The oxygen product recovery and productivity determine the feed pump size and adsorbent volume for a specified production rate.

Table 4. Range of Values of the Dimensionless Groups Used in the Simulations

Dimensionless Group	Range
Π_1	1.42×10^{-5} to 2.27×10^{-2}
Π_2	2.03
Π_3	127.95(5A zeolite); 773.95(Ag-Li-X)
Π_4	6.67×10^{-5} to 5×10^{-3}
Π_5	0.115(5A zeolite); 1.17(Ag-Li-X)
Π_6	0.0365(5A zeolite); 0.09(Ag-Li-X)
Π_7	2.5–5.5
Π_8	0.79
Π_{11}	6.6

Presentation of the simulations results requires further consideration from the point of user convenience. In the present study, since P_L has been fixed at 1 atm, varying Π_7 effectively means only varying P_H. Similarly, varying Π_1 means only varying d_p since the other parameters in this dimensionless group are fixed by the adsorbent (5A or Ag-Li-X) and gas mixture (oxygen and nitrogen) chosen in the simulations. Hence, instead of making the users calculate the dimensionless group values using the values of the constituent dimensional parameters fixed in the simulations, it is more user-friendly to plot the PPSA process performance indicators as a function of d_p/L $(=\Pi_4)$ for different d_p values for a fixed value of P_H. Such plots for three representative P_H values are given in Figure 5 for 5A zolite. Similarly, the results for Ag-Li-X zeolite are shown in Figure 6. Only the purity and recovery plots are given in Figures 5 and 6. Although not evident from the dimensional analysis presented in the Appendix, it was found that productivities correlate very well with another dimensionless group that contains all the three process parameters. This advantage has been exploited in the next section to package the productivity data in a way that allows direct determination of required adsorbent volume for a specified production rate.

In Figures 5 and 6, for a chosen P_H *and* d_p, a change in d_p/L quantifies the effect of a change in bed length on oxygen purity and corresponding recovery. Similarly, for chosen P_H *and* d_p/L, the figures show the effect of a change in d_p on oxygen purity and recovery. It is clear that for some d_p

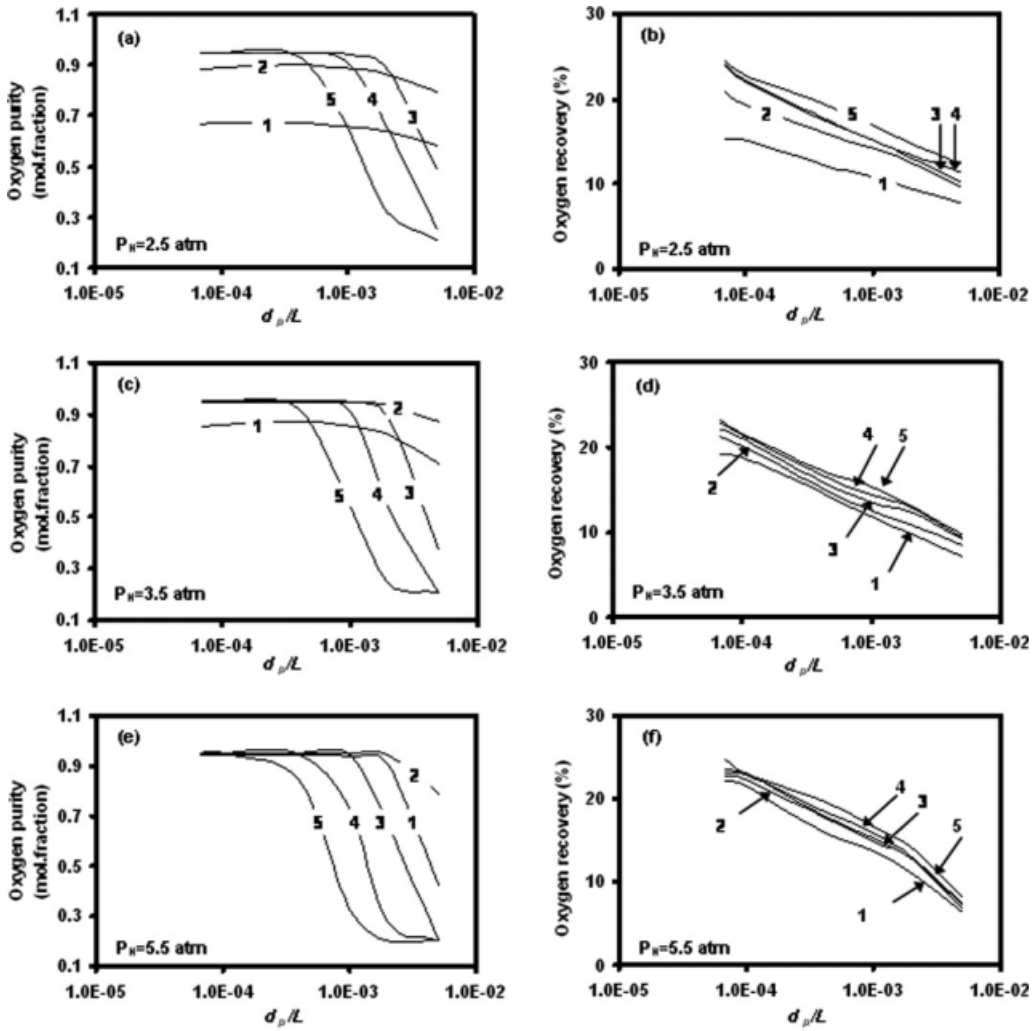

Figure 5. Design plots for PPSA air separation on 5A zeolite relating the process variables to oxygen product purity and recovery.

Optimum adsorption and desorption step durations were used for every combination of process variables. The numbers 1–5 in the plots are for d_p values of 0.001, 0.002, 0.01, 0.02, and 0.04 cm, respectively.

values covered in this investigation there is a critical bed length below which the oxygen purity drops drastically. An optimum in oxygen purity with respect to d_p is also evident from the figures. For the PPSA cycle investigated in this study, oxygen product purity in Ag-Li-X zeolite is lower compared to that in 5A zeolite for the same set of process parameters. In the domain of investigation, oxygen recovery is in the range 10–25% in 5A and in Ag-Li-X zeolite the recovery varies from10 to 55%.

Correlation for the optimum adsorption and desorption times

It has been discussed in the ''Optimum in adsorption time and desorption time'' section that for every combination of operating parameters there is an optimum combination of adsorption and desorption step durations at which the oxygen purity is maximum. How the adsorption and desorption step durations have been optimized for several parameter combinations subsequently simulated to study the PPSA process performance is also detailed in the ''Optimum in adsorption time and desorption time'' section. The semiempirical approach described below gives a dimensionless correlation that relates the optimum adsorption and desorption step durations to the operating process variables (P_H, d_p, and L).

For equilibrium-controlled adsorption the optimum adsorption time, $(t_a)_{theo}$, can be estimated from the residence time of the adsorption wave in the adsorber:

$$(t_a)_{theo} = \frac{L}{\omega} \tag{25}$$

where L is the adsorber length and ω is the adsorption wave velocity. For a trace-component system that follows a linear adsorption isotherm, the adsorption wave velocity in an initially clean bed is given by

$$\omega = \frac{\overline{u}_z}{\left[1 + \frac{(1-\varepsilon)}{\varepsilon} K\right]} \tag{26}$$

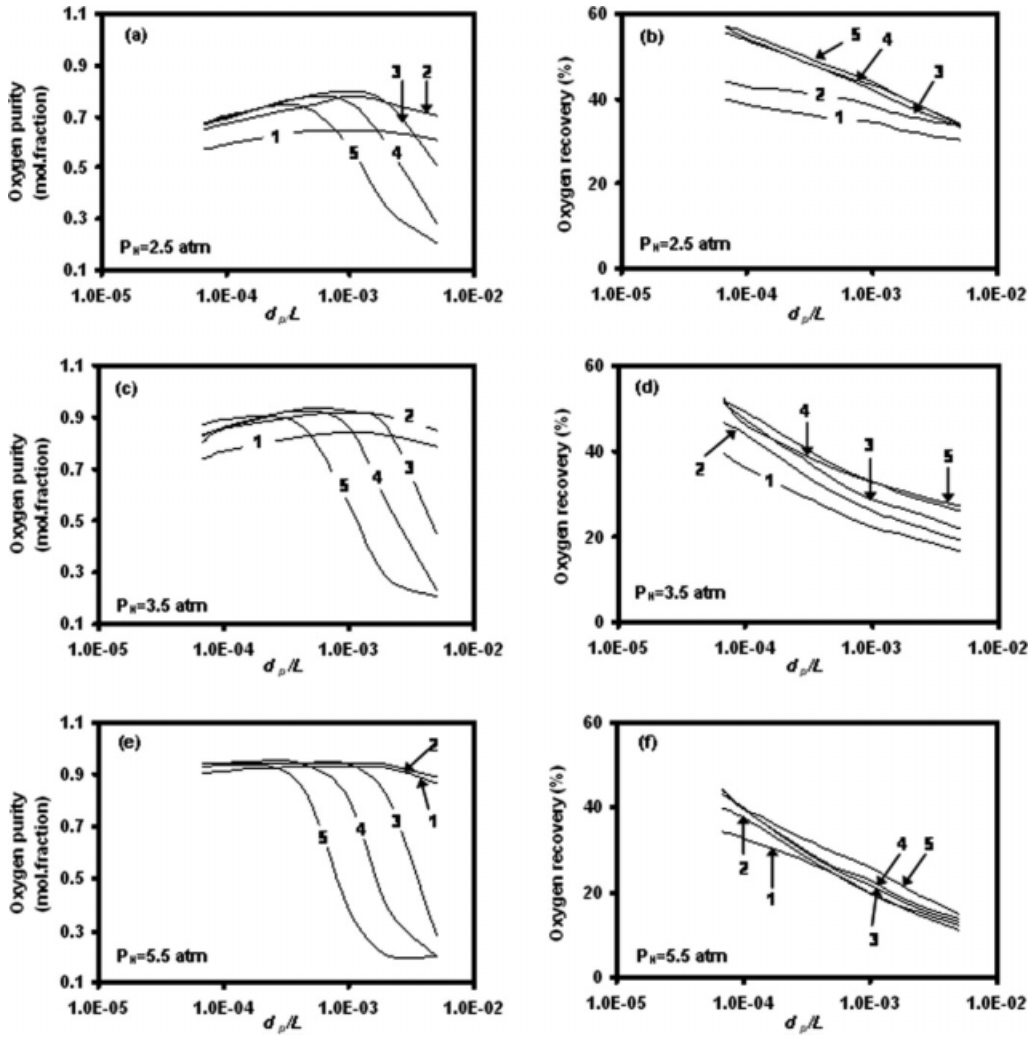

Figure 6. Design plots for PPSA air separation on Ag-Li-X zeolite relating the process variables to oxygen product purity and recovery.

Optimum adsorption and desorption step durations were used for every combination of process variables. The numbers 1–5 in the plots are for d_p values of 0.001, 0.002, 0.01, 0.02, and 0.04 cm, respectively.

where $\overline{u}_z$ is the interstitial gas velocity and K is the dimensionless Henry's law constant. A trace-component system implies a very small amount of adsorbate in the feed such that the equilibrium relationship is linear and the change in velocity due to adsorption is negligible. For such a system Darcy's law in combination with the Blake-Kozeny equation (Eqs. 9 and 10) relates the interstitial velocity to the adsorber length, adsorbent particle diameter, bed voidage, and imposed pressure drop. When Eqs. 9 and 10 are substituted into Eq. 26, the following equation is obtained:

$$\frac{(t_a)_{\text{theo}}}{\left[1+\left(\frac{1-\varepsilon}{\varepsilon}\right)K\right]} = \frac{150}{\frac{\Delta P d_p^2}{\mu L^2}\left(\frac{\varepsilon}{1-\varepsilon}\right)^2} \tag{27}$$

which may be further rearranged to the following form:

$$\frac{\frac{P_L}{\mu}(t_a)_{\text{theo}}}{\left[1+\left(\frac{1-\varepsilon}{\varepsilon}\right)K\right]} = \frac{150}{\left(\frac{P_H}{P_L}-1\right)\frac{d_p^2}{L^2}\left(\frac{\varepsilon}{1-\varepsilon}\right)^2} \tag{28}$$

Equation 28 has the general form

$$Y = \frac{150}{X} \tag{29}$$

where

$$Y = \frac{\frac{P_L}{\mu}(t_a)_{\text{theo}}}{\left[1+\left(\frac{1-\varepsilon}{\varepsilon}\right)K\right]} \equiv \frac{\Pi_9}{[1+\Pi_2 K]} \quad \text{and}$$

$$X = \left(\frac{P_H}{P_L}-1\right)\frac{d_p^2}{L^2}\left(\frac{\varepsilon}{1-\varepsilon}\right)^2 \equiv (\Pi_7-1)\left(\frac{\Pi_4}{\Pi_2}\right)^2$$

Π_2,Π_4, Π_7, and Π_9 are the same dimensionless groups defined in the Appendix.

To examine if the optimum adsorption time normalized with respect to bed capacity in a PPSA system involving a nonlinear adsorption isotherm and bulk separation can be similarly correlated to the process parameters, Y was modified according to the following equation to account for a

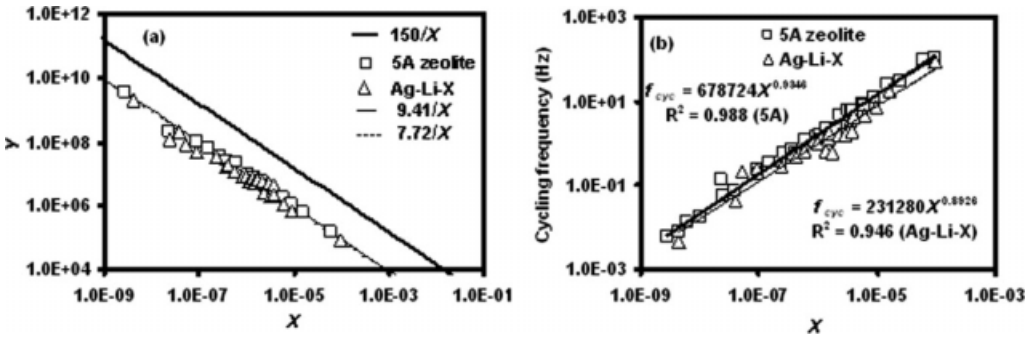

Figure 7. Correlations for relating (a) optimum adsorption step duration and (b) cycling frequency to the dimensionless group *X* which combines the PPSA process parameters.

Results for both 5A and Ag-Li-X are shown.

binary feed mixture following an extended Langmuir isotherm and plotted against X:

$$Y = \frac{\Pi_9}{1 + \Pi_2 \frac{q_{avg}}{c_{avg}}} \quad \text{where}$$

$$\frac{q_{avg}}{c_{avg}} = \frac{q^{\infty} b_A}{1 + b_A \frac{P_{avg} y_{Af}}{RT} + b_B \frac{P_{avg}(1-y_{Af})}{RT}} \quad \text{and} \quad P_{avg} = \frac{(P_H + P_L)}{2}$$

In the aforementioned equations $\frac{q_{avg}}{c_{avg}}$ can be written in terms of the dimensionless groups as follows:

$$\frac{q_{avg}}{c_{avg}} = \frac{K_A}{1 + 0.5\Pi_5\Pi_8(\Pi_7 + 1) + 0.5\Pi_6(1 - \Pi_8)(\Pi_7 + 1)} \tag{30}$$

In the aforementioned equation A denotes the more strongly adsorbed component, nitrogen; q_{avg} is the equilibrium concentration of nitrogen at the average pressure P_{avg} in the bed corresponding to the nitrogen concentration in the feed. The plots are shown in Figure 7a. It is interesting to note that the optimized adsorption times obtained from the simulation for air separation by PPSA on 5A and Ag-Li-X indeed are correlated by an equation similar to Eq. 28 that was derived for a trace-component system obeying a linear adsorption isotherm. The correlations are $Y = 9.41/X$ for the 5A zeolite and $Y = 7.72/X$ for the Ag-Li-X zeolite. The constants 9.41 and 7.72 can be in viewed as empirical compensations for the isotherm nonlinearity, change in velocity due to adsorption, and the effect of residual bed loading on the wave velocity. The cycling frequency obtained from the optimized adsorption and desorption times was also plotted against X and the results along with the correlations are shown in Figure 7b.

As the equilibrium capacities of oxygen and nitrogen in the two adsorbents are significantly different, the closeness of the correlations in Figure 7a suggests the possibility of an adsorbent-independent approximate correlation between Y and X.

By evaluating the appropriate dimensionless groups constituting the variables X and Y, the optimum adsorption time and cycling frequency can be obtained directly either from Figures 7a, b or from the correlations included in these figures for both adsorbents. The optimum desorption time can then be easily calculated from the known optimum adsorption time and cycling frequency. Proper selection of the adsorption and desorption times based on the availability of commercially available cycling valves and pumps is an important consideration for the miniaturization of an oxygen concentrator to meet the needs of active patients with COPD.

To complete the sizing of a PPSA process, the necessary amount of adsorbent must be determined, which is related to the productivity by the following equation:

$$\text{Adsorbent volume (cc)} = \frac{\text{Oxygen delivery rate (cc of oxygen/h)}}{\text{Oxygen productivity (cc of oxygen/cc of adsorbent/h)}} \tag{31}$$

The calculated adsorbent volume for an oxygen delivery rate of 5 LPM is plotted as a function of X in Figure 8 give excellent correlations for both adsorbents. Oxygen concentration in the product stream is dependent on the chosen process parameters according to the correlations in Figures 5 and 6. It is useful to recall that AMA requires $\geq$90% oxygen at a rate of 5 LPM for personal medical applications.

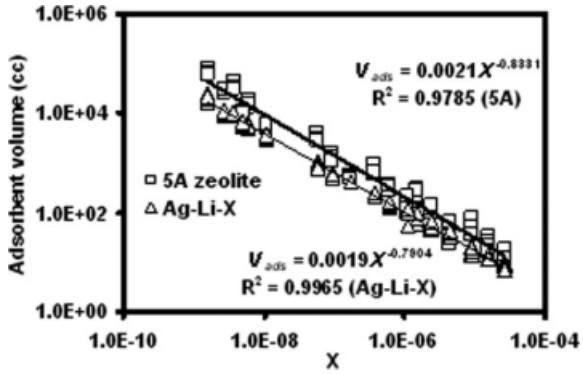

Figure 8. Correlation relating adsorbent volume to the dimensionless group *X* in order to deliver 5 LPM of oxygen at a level of oxygen purity chosen in Figure 5 or 6.

Correlations for 5A and Ag-Li-X zeolites are shown.

Table 5. Design Table for a PPSA Oxygen Concentrator

Oxygen Purity* (mol. fraction)			Adsorption Time (s)		Cycling Frequency (Hz)		Adsorbent Volume (cc)		Weight of Adsorbent (g)	
5A	Ag-Li-X	Bed Length (cm)	5A	Ag-Li-X	5A	Ag-Li-X	5A	Ag-Li-X	5A	Ag-Li-X
0.92	0.89	0.7	0.009	0.017	7.48	4.25	55.2	29.6	66.2	35.6
0.93	0.90	0.8	0.011	0.022	5.82	3.35	69.0	36.6	82.8	44.0
0.93	0.90	0.9	0.014	0.028	4.67	2.71	83.9	44.1	100.7	53.0
0.94	0.91	1	0.018	0.034	3.8	2.25	100.0	52.1	120.0	62.6
0.95	0.92	2	0.071	0.137	1.05	0.65	317.5	155.9	381.0	187.4
0.95	0.91	3	0.160	0.308	0.49	0.32	624.0	295.9	748.8	355.7
0.95	0.91	4	0.284	0.548	0.29	0.19	1007.7	466.3	1209.2	560.5
0.95	0.91	5	0.444	0.857	0.19	0.13	1461.5	663.6	1753.8	797.6
0.95	0.90	10	1.777	3.428	0.05	0.04	4638.5	1984.9	5566.2	2385.8

*Rounded to two decimal places.
$P_H = 3.5$ atm; $d_p = 0.002$ cm; Oxygen delivery rate = 5 LPM.

Since the cycling frequency increases with increasing X, it is now clear that within the range of process parameters required to ensure high ($\geq$90%) product purity, the reduction in size of a pulsed pressure-swing adsorber depends on how fast the process can be cycled.

General Design Procedure

Based on the results in Figures 5–8, a generalized design procedure can be proposed for the production of an enriched oxygen stream from air at an oxygen flow rate of 5 LPM:

(1) Set the design specification for oxygen purity in the product stream.

(2) Select appropriate values of P_H, d_p, and d_p/L from Figure 5 or 6 to ensure the specification set in step 1.

(3) Calculate the value of the dimensionless group X corresponding to the process parameters chosen in step 2.

(4) Obtain the optimum adsorption time and cycling frequency from Figures 7a, b, respectively, for the value of X obtained in step 3. If the adsorption step duration is achievable, then proceed to the next design step; otherwise change the dimensionless groups to achieve implementable adsorption step duration. Since the desorption step duration is longer than the adsorption step duration, the latter is the deciding factor.

(5) Calculate the optimum desorption time from the optimum adsorption time and cycling frequency determined in step 4.

(6) Obtain the volume of adsorbent required to produce 5 LPM of oxygen at the desired purity from Figure 8 using the X value calculated from step 3.

A Case Study in Process Miniaturization

The design specification is set as >90% oxygen purity in the product stream delivered at a rate of 5 LPM of oxygen to remain well within the AMA standard. High pressure oxygen concentrators are not suitable for ambulatory use by patients with active COPD due to the potential hazards associated a high pressure system. Therefore, the maximum pressure that can be used in the design of an oxygen concentrator is limited to few atmospheres above the ambient pressure. Similarly, the (high) frequency of the available valves limits the choice of adsorbent particle size. Prompted by these considerations, an adsorbent particle diameter of 0.002 cm and a pressure drop of 2.5 atm were chosen; possible combinations of bed length and cycling frequency were then explored for both 5A and Ag-Li-X adsorbents. Selected results are summarized in Table 5, which illustrate the role of cycling frequency in PPSA process miniaturization.

Conclusions

A mathematical model for a two-step pulsed pressure swing adsorption (PPSA) process was developed from first principles and the process performance was analyzed successfully by solving the dynamic model equations using COMSOL Multiphysics software. COMSOL Multiphysics together with MATLAB facilitate observing the transient profiles within a single cycle, which are useful for understanding the PPSA process behavior.

PPSA air separation on 5A and Ag-Li-X zeolites has been thoroughly investigated. For both adsorbents the oxygen product purity is a maximum for a combination of operating parameters at unique optimum adsorption and desorption times. The optimum desorption time is longer than the optimum adsorption time to ensure proper regeneration of the bed. These optima arise owing to the self-purging of the bed with the low velocity and high purity desorbed oxygen from the region ahead of adsorption front.

The results from extensive simulations covering a wide range of operating conditions have been consolidated in three design plots (Figures 5 or 6, 7, and 8) for PPSA air separation on 5A and Ag-Li-X zeolites that allow direct determination of the required process parameters (while considering the practical limitations on each of them) and adsorbent volume in order to achieve desired oxygen purity at an oxygen delivery rate of 5 LPM. For the same combination of process parameters 5A zeolite gives higher oxygen product purity but lower recovery (and hence higher adsorbent volume) compared to Ag-Li-X zeolite.

The extent of miniaturization of an oxygen concentrator operated on a PPSA cycle is constrained by the upper limit of rapid cycling that is practically achievable. A significant reduction in size is feasible using commercially available nitrogen-selective adsorbents while keeping the cycling within implementable operating conditions and satisfying AMA specification of $\geq$90% pure oxygen at a rate of 5 LPM.

Acknowledgments

This work was carried out under the research project R279000231112 funded by the Ministry of Education, Singapore.

Notation

$a - t_a$ = cyclic steady-state oxygen profile at the end of the adsorption step for an adsorption step duration indicated by the number in Figure 4
$a - t_d$ = cyclic steady-state oxygen profile at the end of the adsorption step for a desorption step duration indicated by the number in Figure 4
b_i = Langmuir constants for component i, cc/mol
c = total gas phase molar concentration, mol/cc
c_i = molar concentrations of component i in gas phase, mol/cc
c_{avg} = average molar concentration of component A in feed gas at P_{avg}, mol/cc
c_0 = initial molar concentration of component i in feed gas, mol/cc
$d - t_a$ = cyclic steady-state oxygen profile at the end of the desorption step for an adsorption step duration indicated by the number in Figure 4
$d - t_d$ = cyclic steady-state oxygen profile at the end of the desorption step for a desorption step duration indicated by the number in Figure 4
D_L = axial dispersion coefficient, cm^2/s
D_M = molecular diffusivity at average column pressure (P_{avg}) and 25°C, cm^2/s
D_p = macropore diffusivity, cm^2/s
d_p = adsorbent particle size, cm
f_{cyc} = cycling frequency, s^{-1}
K_i = Henry's law constant for component i, $(mol/cc)_{solid\ phase}/(mol/cc)_{gas\ phase}$
k_i = effective mass transfer coefficients for component i, s^{-1}
k_f = external gas film mass transfer coefficient, cm/s
k_p = bed permeability, cm^2
L = bed length, cm
n = number of cycles completed
N_i = molar flux of component i with respect to fixed coordinates, $mol/cm^2 \cdot s$
P = total pressure, atm
P_H = total pressure at $z = 0$ during adsorption step, atm
P_L = total pressure at $z = L$ during adsorption and $z = 0$ during desorption, atm
P_{avg} = average of inlet and outlet total pressures during adsorption, atm
ΔP = pressure difference between the inlet and outlet of column, atm
p_i = partial pressure of component i, atm
q_{avg} = average adsorbed phase concentration of component A at P_{avg}, mol/cc
$\overline{q}_i$ = average adsorbed phase concentration of component i in the particle, mol/cc
q_i^e = equilibrium adsorbed phase concentration of component i, mol/cc
q_0 = equilibrium adsorbed phase concentration corresponds to c_0, mol/cc
q^∞ = saturation constant, mol/ cc
R = universal gas constant, atm·cc/mol·K
r_p = adsorbent particle radius, cm
T = temperature, K
t = time, s
t_a = adsorption time, s
t_d = desorption time, s
u_z = gas phase velocity through porous media in z-direction, cm/s
$\overline{u}_z$ = average gas velocity from Blake-Kozney equation, cm/s
V_{ads} = adsorbent volume, cc
X = dimensionless function defined by Eq. 28
Y = dimensionless function defined by Eq. 28
y_i = mole fraction of component i
y_{i0} = mole fraction of component i in feed
z = axial distance, cm
∞ = saturation

Greek letters

ε = bed voidage
ε_p = particle voidage
γ_1, γ_2 = constants in equation for axial dispersion coefficient
μ = viscosity of gas at room temperature, atm s
θ = dimensionless adsorption time, $\frac{\varepsilon_p D_p}{r_p^2}\left(\frac{c_0}{q_0}\right)t_a$
τ = tortuosity factor
ω = adsorption wave velocity, cm/s
$\Pi_1 - \Pi_{11}$ = dimensionless groups defined by Eqs. A15–A25 in the Appendix
Ω = linear driving force model parameter

Subscripts/ superscripts/abbreviations

A = nitrogen
a = adsorption step
ads = adsorbent
avg = average
B = oxygen
current = current value
cyc = cycle
d = desorption step
e = equilibrium value
H = high pressure
i = component A or B
L = low pressure
p = particle
ref = reference value
theo = theoretically calculated value
z = axial direction
0 = feed gas
* = dimensionless variable
+ = just inside
− = just outside

Literature Cited

1. Turnock PH, Kadlec RH. Separation of nitrogen and methane via periodic adsorption. *AIChE J*. 1971;17:335–342.
2. Jones RL, Keller GE. Rapid pressure swing adsorption processes with high enrichment factor. *U.S. Pat*. 4,194,892, 1980.
3. Pritchard CL, Simpson GK. Design of an oxygen concentrator using the rapid pressure-swing adsorption principle. *Chem Eng Res Des*. 1986;64:467–472.
4. Sircar S. Gas separation by rapid pressure swing adsorption. *U.S. Pat*. 5,071,449, 1991.
5. Hart J, Thomas WJ. Gas separation by pulsed pressure swing adsorption. *Gas Sep Purif*. 1991;5:125–133.
6. Alpay E, Kenney CN, Scott DM. Simulation of rapid pressure swing adsorption and reaction processes. *Chem Eng Sci*. 1993;48:3173–3185.
7. Baron G. Modeling of PSA processes. *Gas Sep Purif*. 1993;7:111–117.
8. Lu ZP, Loureiro JM, Rodrigues AE, Levan MD. Simulation of a 3-Step one-column pressure swing adsorption process. *AIChE J*. 1993;39:1483–1496.
9. Alpay E, Kenney CN, Scott DM. Adsorbent particle-size effects in the separation of air by rapid pressure swing adsorption. *Chem Eng Sci*. 1994;49:3059–3075.
10. Kulish S, Keller RP. Rapid cycle pressure swing adsorption oxygen concentrator method and apparatus. *U.S. Pat*. 5,827,358, 1998.
11. Zhang Z, Guan J, Ye Z. Separation of a nitrogen-carbon dioxide mixture by rapid pressure swing adsorption. *Adsorption*. 1998;4:173–177.
12. Ackley MW, Zhong G. Medical oxygen concentrator. *U.S. Pat*. 6,551,384 B1, 2003.
13. Huang WC, Chou CT. Comparison of radial- and axial-flow rapid pressure swing adsorption processes. *Ind Eng Chem Res*. 2003;42:1998–2006.
14. Todd RS, Webley PA. Mass-transfer models for rapid pressure swing adsorption simulation. *AIChE J*. 2006;52:3126–3144.
15. Keefer BG, Mclean CR, Babicki ML. Life support oxygen concentrator. *U.S. Pat*. 7,250,073 B2, 2007.
16. Khiavi SA, Sawada JA, Gibbs AC, Alvaji J. Rapid cycle syngas pressure swing adsorption system. *U.S. Pat*. 0,125,228 A1, 2007.
17. Warren JL. Miniaturized wearable oxygen concentrator. *U.S. Pat*. 6,478,850 B2, 2002.

18. Warren JL. Miniaturized wearable oxygen concentrator. *U.S. Pat.* 6,547,851 B2, 2003.
19. Kopaygorodsky EM, Guliants VV, Krantz WB. Predictive dynamic model of single-stage ultra-rapid pressure swing adsorption. *AIChE J*. 2004;50:953–961.
20. Jee JG, Lee JS, Lee CH. Air separation by a small-scale two-bed medical O_2 pressure swing adsorption. *Ind Eng Chem Res*. 2001;40:3647–3658.
21. Jee,JG, Kim MB, Lee CH. Pressure swing adsorption processes to purify oxygen using a carbon molecular sieve. *Chem Eng Sci*. 2005;60:869–882.
22. Kikkinides ES, Yang RT. Effects of bed pressure drop on isothermal and adiabatic adsorber dynamics. *Chem Eng Sci*. 1993;48:1545–1555.
23. Yang J, Park MW, Chang JW, Ko SM, Lee CH. Effect of pressure drop in a PSA process. *Koren J Chem Eng*. 1998;15:211–216.
24. Yang J, Lee CH. Adsorption dynamics of a layered bed PSA for H_2 recovery from coke oven gas. *AIChE J*. 1998;44:1325–1333.
25. Jee JG, Lee SJ, Kim MB, Lee CH. Three-bed PVSA processes for high-purity O_2 generation from ambient air. *AIChE J*. 2005;51:2988–2999.
26. Farooq S, Ruthven DM, Boniface HA. Numerical simulation of a pressure swing adsorption oxygen unit. *Chem Eng Sci*. 1989;44:2809–2816.
27. Hutson ND, Rege SU, Yang RT. Mixed cation zeolites: Li_xAg_y-X as a superior adsorbent for air separation. *AIChE J*. 1999;45:724–734.
28. Ruthven DM, Farooq S, Knaebel KS. *Pressure Swing Adsorption*. New York: VCH Publishers, 1994.
29. Raghavan NS, Hassan MM, Ruthven DM. Numerical simulation of a PSA system using a pore diffusion model. *Chem Eng Sci*. 1986;41:2787–2793.
30. Bird RB, Stewart WE, Lightfoot EN. *Transport Phenomena*. New York: Wiley, 1960.
31. Ruthven DM. *Principles of Adsorption and Adsorption Processes*. New York: Wiley, 1994.
32. Todd RS, Webley PA. Limitations of the LDF/equimolar counterdiffusion assumption for mass transport within porous adsorbent pellets. *Chem Eng Sci*. 2002;57:4227–4242.
33. Krantz WB. *Scaling Analysis in Modeling Transport and Reaction Processes*. New York: Wiley, 2007.

Appendix: Dimensionless Equations

Equations 5–9 and 12–20 were made dimensionless by introducing the following dimensionless variables.

$$P^* \equiv \frac{P}{P_L};\ p_A^* \equiv \frac{p_A}{P_L};\ \bar{q}_A^* \equiv \frac{\bar{q}_A}{q^\infty};\ \bar{q}_B^* \equiv \frac{\bar{q}_B}{q^\infty};$$
$$q_A^{e^*} \equiv \frac{q_A^*}{q^\infty};\ q_B^{e^*} \equiv \frac{q_B^*}{q^\infty};\ k_A^* \equiv \frac{\tau d_p^2 q^\infty P_{avg} b_A k_A}{60\varepsilon_p P_L D_M};$$
$$k_B^* \equiv \frac{\tau d_p^2 q^\infty P_{avg} b_B k_B}{60\varepsilon_p P_L D_M};\ t^* \equiv \frac{d_p^2 P_L t}{150\mu L^2}\left(\frac{\varepsilon}{1-\varepsilon}\right)^2;$$
$$z^* \equiv \frac{z}{L};\ u_z^* \equiv \frac{150 u_z \mu L}{d_p^2 P_L}\left(\frac{1-\varepsilon}{\varepsilon}\right)^2$$

Substituting these dimensionless variables in the aforementioned equations results in the following dimensionless equations:

$$\frac{\partial p_A^*}{\partial t^*} = \Pi_1\left[0.7\frac{1}{(\Pi_7+1)} + 0.5\frac{\Pi_7}{\Pi_1}\left(1-\frac{1}{\Pi_7}\right)\Pi_4\right] \frac{\partial}{\partial z^*}\left[P^*\frac{\partial}{\partial z^*}\left(\frac{p_A^*}{P^*}\right)\right] - \frac{\partial}{\partial z^*}\left(p_A^* u_z^*\right) - \Pi_2\Pi_3\frac{\partial \bar{q}_A^*}{\partial t^*} \quad \text{(A1)}$$

$$\frac{\partial P^*}{\partial t^*} = -\frac{\partial}{\partial z^*}\left(P^* u_z^*\right) - \Pi_2\Pi_3\frac{\partial}{\partial t^*}\left(\bar{q}_A^* + \bar{q}_B^*\right) \quad \text{(A2)}$$

$$u_z^* = -\frac{\partial P^*}{\partial z^*} \quad \text{(A3)}$$

$$\frac{\partial \bar{q}_A^*}{\partial t^*} = \frac{\Pi_{11}}{(1+\Pi_7)}\frac{\Pi_1}{\Pi_4^2}\frac{1}{\Pi_3\Pi_5}k_A^*\left(q_A^{e^*} - \bar{q}_A^*\right) \quad \text{(A4)}$$

$$\frac{\partial \bar{q}_B^*}{\partial t^*} = \frac{\Pi_{11}}{(1+\Pi_7)}\frac{\Pi_1}{\Pi_4^2}\frac{1}{\Pi_3\Pi_6}k_B^*\left(q_B^{e^*} - \bar{q}_B^*\right) \quad \text{(A5)}$$

$$q_A^{e^*} = \Pi_5\frac{p_A^*}{1+\Pi_5 p_A^* + \Pi_6\left(P^* - p_A^*\right)} \quad \text{(A6)}$$

$$q_B^{e^*} = \Pi_6\frac{P^* - p_A^*}{1+\Pi_5 p_A^* + \Pi_6\left(P^* - p_A^*\right)} \quad \text{(A7)}$$

$$k_A^* = \left[1 + \Pi_5 p_A^* + \Pi_6\left(P^* - p_A^*\right)\right] \quad \text{(A8)}$$

$$k_B^* = \left[1 + \Pi_5 p_A^* + \Pi_6\left(P^* - p_A^*\right)\right] \quad \text{(A9)}$$

$$\left.\begin{array}{l} P^*\frac{\partial}{\partial z^*}\left(\frac{p_A^*}{P^*}\right) = \frac{1}{\Pi_1\left[0.7\frac{1}{(\Pi_7+1)}+0.5\frac{\Pi_7}{\Pi_1}\left(1-\frac{1}{\Pi_7}\right)\Pi_4\right]}\frac{\partial P^*}{\partial z^*}\left(\Pi_7\Pi_8 - p_A^*\right) \\ P^* = \Pi_8 \end{array}\right\} \text{at} \quad z^* = 0^+ \quad \frac{1}{150}\left(\frac{\Pi_4}{\Pi_2}\right)^2 n(\Pi_9+\Pi_{10}) \le t^* \le \frac{1}{150}\left(\frac{\Pi_4}{\Pi_2}\right)^2[(n+1)\Pi_9 + n\Pi_{10}] \quad \text{(A10)}$$

$$\left.\begin{array}{l} \frac{\partial}{\partial z^*}\left(\frac{p_A^*}{P^*}\right) = 0 \\ P^* = 1 \end{array}\right\} \text{at} \quad z^* = 0^+ \quad \frac{1}{150}\left(\frac{\Pi_4}{\Pi_2}\right)^2[(n+1)\Pi_9 + n\Pi_{10}] \le t^* \le \frac{1}{150}\left(\frac{\Pi_4}{\Pi_2}\right)^2(n+1)(\Pi_9+\Pi_{10}) \quad \text{(A11)}$$

$$\left.\begin{array}{l} \frac{\partial}{\partial z^*}\left(\frac{p_A^*}{P^*}\right) = 0 \\ P^* = 1 \end{array}\right\} \text{at} \quad z^* = 1^- \quad \frac{1}{150}\left(\frac{\Pi_4}{\Pi_2}\right)^2 n(\Pi_9+\Pi_{10}) \le t^* \le \frac{1}{150}\left(\frac{\Pi_4}{\Pi_2}\right)^2[(n+1)\Pi_9 + n\Pi_{10}] \quad \text{(A12)}$$

$$\left.\begin{array}{l} \frac{\partial}{\partial z^*}\left(\frac{p_A^*}{P^*}\right) = 0 \\ \frac{\partial P^*}{\partial z^*} = 0 \end{array}\right\} \text{at} \quad z^* = 1^- \quad \frac{1}{150}\left(\frac{\Pi_4}{\Pi_2}\right)^2[(n+1)\Pi_9 + n\Pi_{10}] \le t^* \le \frac{1}{150}\left(\frac{\Pi_4}{\Pi_2}\right)^2(n+1)(\Pi_9+\Pi_{10}) \quad \text{(A13)}$$

$$\left.\begin{array}{l} p_A^* = \Pi_8 \\ P^* = 1 \\ \bar{q}_A^* = q_A^{e^*}\Big|_{p_A^*} \\ \bar{q}_B^* = q_B^{e^*}\Big|_{p_B^*} \end{array}\right\} \quad \text{at} \quad t^* = 0, \quad 0 \le z^* \le 1 \quad \text{(A14)}$$

The dimensionless groups in the aforementioned dimensionless equations are defined as follows:

$$\Pi_1 = \frac{150\mu D_M}{d_p^2 P_L}\left(\frac{1-\varepsilon}{\varepsilon}\right)^2 \quad \text{(A15)}$$

$$\Pi_2 \equiv \frac{1-\varepsilon}{\varepsilon} \quad \text{(A16)}$$

$$\Pi_3 \equiv \frac{RTq^{\infty}}{P_L} \quad \text{(A17)}$$

$$\Pi_4 = \frac{d_p}{L} \quad \text{(A18)}$$

$$\Pi_5 \equiv \frac{b_A}{RT} P_L \quad \text{(A19)}$$

$$\Pi_6 \equiv \frac{b_B}{RT} P_L \quad \text{(A20)}$$

$$\Pi_7 \equiv \frac{P_H}{P_L} \quad \text{(A21)}$$

$$\Pi_8 \equiv y_{A0} \quad \text{(A22)}$$

$$\Pi_9 = \frac{t_a P_L}{\mu} \quad \text{(A23)}$$

$$\Pi_{10} = \frac{t_d P_L}{\mu} \quad \text{(A24)}$$

$$\Pi_{11} = \frac{60\varepsilon}{\tau} \quad \text{(A25)}$$

Hence, the oxygen product purity, recovery and productivity will be a function of dimensionless groups defined in equations A15–A25; that is,

$$\left.\begin{array}{l}\text{Oxygen purity}\\ \text{Oxygen recovery}\\ \text{Productivity}\end{array}\right\} \equiv f(\Pi_1, \Pi_2, \Pi_3, \Pi_4, \Pi_5, \Pi_6, \Pi_7, \Pi_8, \Pi_9, \Pi_{10}, \Pi_{11}) \quad \text{(A26)}$$

For air separation using a specified adsorbent, operating pressures and temperature, the oxygen product purity, recovery and productivity are only a function of five dimensionless groups; the remaining dimensionless groups are dependent on adsorbent properties, feed gas mole fraction and operation pressure, and temperature. Therefore, for air separation using a specific adsorbent it follows that

$$\left.\begin{array}{l}\text{Oxygen purity}\\ \text{Oxygen recovery}\\ \text{Productivity}\end{array}\right\} \equiv f(\Pi_1, \Pi_4, \Pi_7, \Pi_9, \Pi_{10}) \quad \text{(A27)}$$

If the oxygen product purity is maximized with respect to the durations of the adsorption and desorption steps, two additional independent equations are generated that can be used to eliminate the dimensionless groups Π_9,Π_{10}. Hence, the oxygen product purity, recovery and productivity mainly will depend on only three dimensionless groups namely Π_1,Π_4,Π_7.

$$\left.\begin{array}{l}\text{Oxygen purity}\\ \text{Oxygen recovery}\\ \text{Productivity}\end{array}\right\} \equiv f(\Pi_1, \Pi_4, \Pi_7) \quad \text{(A28)}$$

Therefore, from the above equation, the effect of process parameters, bed length and particle size, can be studied in terms of dimensionless groups Π_1 and Π_4 for a constant value of the other dimensionless group Π_7, which is only a function of the maximum pressure in the cycle.

Manuscript received Mar. 10, 2008, revision received Jan. 26, 2009, and final revision received Apr. 24, 2009.